RSC Advances

PAPER

View Article Online
View Journal | View Issue

Cite this: *RSC Adv.*, 2024, **14**, 12754

Insight into the probability of ethoxy(pentafluoro) cyclotriphosphazene (PFPN) as the functional electrolyte additive in lithium–sulfur batteries†

Ning Li, ‡[a] Yu Zhang, ‡[a] Shun Zhang,[a] Lu Shi,[b] Jie-Yu Zhang,[a] Ke-Meng Song,[a] Jin-Chun Li*[a] and Fang-Lei Zeng *[a]

Enhancing the flame retardancy of electrolytes and the stability of lithium anodes is of great significance to improve the safety performance of lithium–sulfur (Li–S) batteries. It is well known that the most commonly used ether based electrolyte solvents in Li–S batteries have a lower flash point and higher volatility than the ester electrolyte solvents in Li-ion batteries. Hence, lithium–sulfur batteries have greater safety risks than lithium-ion batteries. Herein, ethoxy(pentafluoro)cyclotriphosphazene (PFPN), which is commonly used as a flame retardant for ester electrolytes in lithium-ion batteries, is utilized as both a film-forming electrolyte additive and a flame retardant additive for the ether electrolyte to investigated its applicability in Li–S batteries. It is found that the ether electrolyte containing PFPN not only has good flame retardant properties and a wide potential window of about 5 V, but also can form a stable SEI film on the surface of a lithium anode. As a result, with the ether-based electrolyte containing 10 wt% PFPN, Li–Cu and Li–S batteries all delivered a stable cycling performance with a high coulombic Efficiency and a long-lifespan performance, which were all superior to the batteries using the ether-based electrolyte without PFPN. This study demonstrates an effective solution to solve the problems of flammable ether-based electrolytes and reactive lithium anodes, and it may contribute to the development of safe Li–S batteries.

Received 8th December 2023
Accepted 5th April 2024

DOI: 10.1039/d3ra08379a

rsc.li/rsc-advances

1. Introduction

At present, the lithium-ion cell has been widely used in communication, transportation and energy storage because of its no memory effect, small self-discharge and long cycle life.[1,2] Although the laboratory energy density of commercial lithium-ion secondary batteries has reached 300–400 W h kg^{-1}, it is difficult to further significantly improve its specific capacity and energy due to its theoretical specific capacity limitations of anode and cathode materials.[3] In this context, the lithium–sulfur (Li–S) cell system has great technical appeal because of its theoretical specific energy density up to 2600 W h kg^{-1} which is several times that of lithium-ion cells.[4] Moreover, sulfur is an abundant, inexpensive and environmentally friendly material, which also brings extra benefit for Li–S batteries.[5] In spite of these advantages, severe safety hazards caused by the flammable ether electrolyte and the highly reactive lithium metal anode still limit the commercial application of Li–S batteries.

In the Li–S cell system, the most commonly used electrolyte solvents are ether solvents such as dimethoxyethane (DME) and 1,3-dioxolane (DOL), which both have a very low flash point (0 °C for DME[6] and 1 °C for DOL[7]) and high volatility. These characteristics of the ether electrolyte solvents determine that there are great safety risks in the use of Li–S cell. For the reactive lithium metal anode, it can easily react with the ether-based electrolytes and soluble intermediate products-polysulfides in Li–S cell, and immediately form a solid electrolyte interphase (SEI) layer on the surface of lithium metal anode.[8] Unfortunately, the SEI layer tends to unstable and fragile, which would cause a serious irreversible capacity degradation. More seriously, the non-uniform electrochemical dissolution/deposition of lithium anode would result in the formation of lithium dendrites, which can penetrate separator and cause serious safety hazards.

To solve these above problems, a large number of brilliant works have been conducted on safer electrolytes for Li–S batteries, such as solid electrolyte, ionic liquid, high concentration electrolyte, fluorinated solvents and flame retardant. Although these works have achieved excellent improvements, they also have obvious defects, such as poor interface compatibility and complicated preparation process (solid electrolyte),[9]

[a]*School of Material Science and Engineering, Jiangsu Collaborative Innovation Center for Photovoltaic Science and Engineering, Jiangsu Province Cultivation base for State Key Laboratory of Photovoltaic Science and Technology, Changzhou University, Changzhou 213164, China. E-mail: fanglei_zeng0802@163.com; ljc999@cczu.edu.cn*
[b]*School of Mechanical Engineering, Jiangsu University, Zhenjiang 212013, China*

† Electronic supplementary information (ESI) available. See DOI: https://doi.org/10.1039/d3ra08379a

‡ These authors contributed equally to this work.

high cost and high viscosity (high concentration electrolyte and ionic liquid),[10,11] low solubility and low ionic conductivity (fluorinated solvents)[12] and other problems. In consideration of the balanced trade-offs between cost, scalability, safety and electrochemical compatibility, adding functional flame retardants to the electrolyte is one of the most straightforwards and effective ways to prevent ignition of electrolyte and stabilize the interface of lithium anode, finally improving the performance of Li–S cells.

At present, commonly used flame retardant additives include trimethyl phosphate (TMP),[13] dimethyl methylphosphonate (DMMP),[14] fluoroethylene carbonate (FEC),[15] tris(2,2,2-trifluoroethyl)phosphate (TFEP)[16] *etc.* Among them, organophosphorus flame retardants are one of the most commonly studied flame retardants are organophosphorus flame retardants. However, these flame retardants are more used in carbonate electrolyte and less used in ether electrolyte. In recent years, due to the rapid development of lithium–metal batteries, the flame retardance of ether electrolyte based on organophosphorus flame retardants has gradually been reported. Among them, phosphazene-based flame retardants are the most reported because phosphazenes are known for their outstanding flame-retarding properties with rich F, N, and P elements. When applied in carbonate-based electrolytes, only 5% phosphazene-based flame retardants can achieve the flame retardance of carbonate-based electrolyte.[17]

Therefore, it is hoped that phosphazenes can improve the flame retardance of ether-based electrolyte. Besides, for ether-based electrolyte, the ether solvents (DOL/DME) have lower dielectric constants, which can achieve good electrolyte miscibility with phosphazene flame retardant without obvious phase separation that occur as the carbonate-based electrolyte mixing with phosphazene flame retardant.[18] Therefore, it is possible to obtain a good flame retardant ether electrolyte with phosphonitrile. More importantly, recent studies have shown that phosphazenes also can form stable LiF and Li_3N-rich SEI layers on the surface of lithium metal anodes and inhibit the formation of dendrite lithium,[19] finally improving the safety of the lithium metal anode. Fei *et al.*[20] also found that phosphazene flame retardant (such as hexafluorocyclotriphosphazene, HFPN) could enhance the electrochemical properties of Li–S cell by reducing the solubility of polysulfides and reducing the electrode interphase resistance. These results suggested that phosphazene flame retardant could be considered as an useful additive for safer lithium sulfur batteries.

In addition, there are many researches on the flame performance of ester electrolyte and few reports on the flame performance of ether electrolyte. Moreover, the research on flame retardancy of ether-based electrolytes suffers from the limitation of using single components or one-sided functions. For instance, solvents mostly employ DME while neglecting DOL. However, DOL plays a crucial role in promoting stable lithium-ion plating/stripping and improving cell self-discharge in Li–S batteries.[21] Additionally, when investigating the mechanism of additives, other additives (such as $LiNO_3$) are commonly included, and the specific effects of individual additive cannot be better demonstrated. Therefore, in this work, the effects of phosphazene additives on the flame retardancy of DOL/DME ether electrolyte and the interface stability of lithium metal anode would be studied in detail. Among the commonly used phosphazene additives, ethoxy(pentafluoro)cyclotriphosphazene (PFPN) demonstrates outstanding flame retardancy, chemical stability and multifunctionality, and its dosage is small.[22] Undoubtedly, it is an ideal flame-retardant additive.

In this study, PFPN was introduced as an additive in DME/DOL ether-based electrolyte. Compared to other flame retardants, PFPN takes full advantage of the gas-phase flame inhibition mechanism and condensed-phase flame inhibition mechanism. That is, PFPN inhibits the chain reaction of substance combustion by reducing the concentration of surrounding oxygen after combustion and trapping free radicals generated during combustion decomposition, thus achieving the flame retardant of ether electrolyte. More importantly, PFPN also could enhance the compactness and smoothness of the SEI layer on the electrode surface, which would benefit for facilitating the platting/stripping behavior of lithium ions, thereby suppressing the growth of lithium dendrites, and enhancing the safety and electrochemical performance of the cell. In a word, PFPN not only has good flame retardant effect on ether electrolyte, but also can form a stable SEI film on the surface of lithium anode (Fig. 1). As a result, with the ether-based electrolyte containing PFPN, Li–Cu and Li–S batteries all delivered a stable cycling performance. In conclusion, the ether-based electrolyte containing PFPN can effectively solve the problems about the flammable ether-based electrolyte and reactive lithium anode simultaneously, which would be benefit for the development of the safe Li–S batteries.

2. Experimental

2.1 Materials

Lithium bis(trifluoromethylulfon)imide (LiTFSI), ethoxy(pentafluoro)cyclotriphosphazene (PFPN), 1,3-dioxolane (DOL), 1,2-

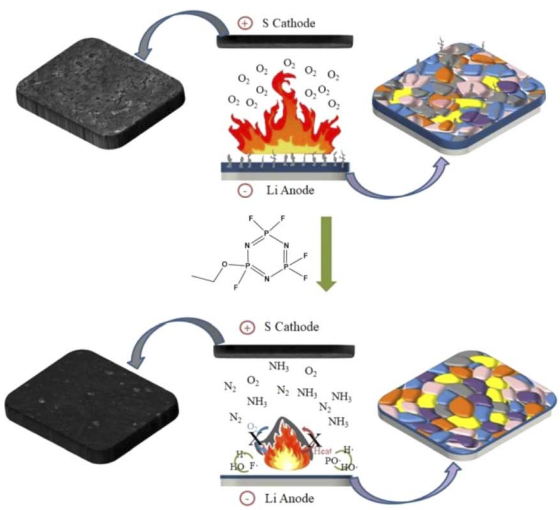

Fig. 1 Schematic diagram of the flame retardant mechanism of PFPN and its influence on the solid electrolyte layer on the electrode surface.

dimethoxyethane (DME) were purchased from DoDo Chemical Technology Co., Ltd. *N*-Methyl-2-pyrrolidone (NMP) was provided by Shanghai Lingfeng Chemical Reagent Co., Ltd. *N*-Propanol was obtained from Aladdin Reagents (Shanghai) Co., Ltd. LA133 was bought from the Sichuan Indigo Materials Science and Technology Group Co., Ltd. Carbon black was provided by Cabot Co., Ltd. Li foil was purchased from the China Energy Lithium (Tianjin) Co., Ltd. Cu foil and aluminum foil was obtained from the HF-Kejing Co., Ltd. Polypropylene (Celgard, 2325) was obtained from the Zhongtian Technology Group Co., Ltd.

2.2 Sample preparation

The electrolyte containing 1.0 M LiTFSI in DOL/DME (v/v = 1/1) without PFPN was used as the basic electrolyte, labeled as PFPN-0. The flame-retardant electrolyte were obtained by made up of PFPN (5%, 10%, 15%, 20% and 25%) in the basic electrolyte, obtaining electrolytes PFPN-5, PFPN-10, PFPN-15, PFPN-20, PFPN-25.

2.3 Preparation of carbon–sulfur cathode

The carbon–sulfur composite material, conductive agent (Super P), and adhesive (LA133) were mixing in a weight ratio of 70 : 20 : 10 in deionized water and *n*-propyl alcohol solution (3 : 1 by volume). Then the obtained slurries were cast on aluminum foil. After being dried in a vacuum oven at 50 °C for 24 h, the electrode was cut and dried again before use. The diameter of the electrode disks was d-14 mm. The sulfur mass load in each electrode is about 2.3 mg cm^{-2}.

2.4 Characterizations

The prepared electrolyte was soaked into the fiberglass membrane and ignited with an alcohol lamp. The flame retardant effect was judged by observing the flame and burning time. The wetting performance of the electrolyte was verified by dropping it onto the separator and utilizing a contact angle measuring device. Long glass fibers were wetted with the electrolyte, and the value of the Limiting Oxygen Index (LOI) was measured using an oxygen index meter. The obtained electrodes were washed with DME before next analysis. The electrode morphologies were observed by scanning electron microscopy (SEM, JSM-IT 100, Hitachi, Japan).

2.5 Electrochemical measurements

2025-type coin cells were all assembled in an argon-filled glove box with Celgard 2325 microporous membranes as separators. Ionic conductivity of the electrolytes was recorded by a conductivity meter (DDB-303A, INESA, Shanghai) at room temperature. The linear sweep voltammetry (LSV) tests were performed on an electrochemical workstation (CHI660E, Chenhua, China) with the scan rate of 1.0 mV s^{-1} to explore the redox behavior of the electrolytes. Electrochemical impedance spectrum (EIS) was measured by a CHI600E with an amplitude of 10 mV in the frequency range from 10^5 to 0.01 Hz. Li–Li symmetrical cells were fabricated by using a Li foil as the working electrode and another Li foil as the counter electrode. The current densities and the related discharge capacities were 0.5 mA cm^{-2} with 0.5 mA h cm^{-2}, and 1.0 mA cm^{-2} with 1.0 mA h cm^{-2} in Li–Li cells. The Li–Cu cells were assembled as the same process excepting using Cu foil as the working electrode. The Li–Cu batteries were tested with constant current densities of 0.2 mA cm^{-2} and 0.5 mA cm^{-2}. The Li–S cells were assembled with the sulfur cathode, lithium metal anode in an argon-filled glove box. The charge–discharge performances were tested in the voltage range of 1.7–2.8 V at the current density of 0.2C (1C = 1675 mA g^{-1}) using a LAND test system (GSV-30L, Wuhan) at room temperature.

3. Results and discussion

The fiberglass membrane are immersed in the prepared electrolytes, and then the flame-retardant performance of the electrolyte is evaluated by measuring the combustion time of the membrane after ignition, as shown in Fig. 2a and Video S1–S6.† The basic electrolyte (PFPN-0) exhibits a strong flame after ignition, and the flame characteristics and combustion time remains basically unchanged after adding 5 wt% PFPN. However, as the PFPN content increased to 10 wt%, 15 wt%, 20 wt% and 25 wt%, the combustion time significantly decreased to 8 s, 7 s, 5 s and 3 s, respectively. In order to further investigate the safety of the electrolytes, the limiting oxygen index (LOI) and self-extinguishing time (SET) tests were performed as shown in Fig. S1 and S2.† It can be observed that with the increase of PFPN addition from 0 wt% to 5 wt%, 10 wt% and 15 wt%, the LOI value of electrolyte significantly increased from

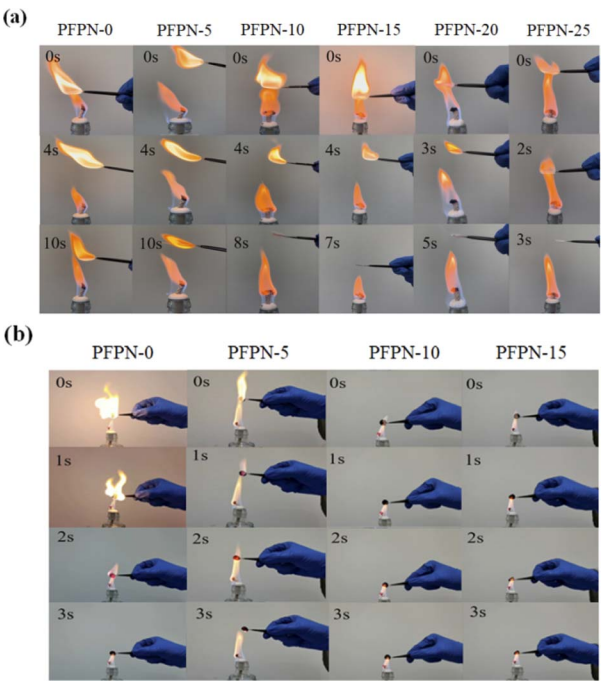

Fig. 2 Combustion tests of (a) fiberglass membranes and (b) cycled sulfur cathodes after 50 cycles with ether-based electrolytes containing PFPN (PFPN-0, PFPN-5, PFPN-10, PFPN-15, PFPN-20, PFPN-25).

14 to 17, 19 and 22, while the SET value significantly decreased from 147.9 to 108.2, 68.6 and 53.3, and finally reached 20 and 0. These results indicate that PFPN can effectively enhance the flame retardancy of the PFPN-0 electrolyte. To examine the flame performance of PFPN in Li–S batteries, the combustion test of the cycled sulfur cathodes after 50 cycles are carried out as shown in Fig. 2b. The cycled sulfur cathodes using the basic electrolyte and PFPN-5 electrolyte are all ignited quickly but extinguished after 3 s. However, the cycled sulfur cathodes using PFPN-10 electrolyte and PFPN-15 electrolyte are rapidly extinguished after ignition (<1 s). These findings suggest that the flame retardant effects of PFPN is benefit from the synergistic interaction between the condensed phase flame retardant mechanism and the free radical trapping mechanism. During combustion, the formation of carbon layers on the surface of phosphorus compounds could effectively hinder the supply of oxygen and reduce the concentration of combustible gases.[23] Additionally, the hydrogen radical (H$^{\bullet}$) and hydroxyl radical (HO$^{\bullet}$) generated from PFPN decomposition could be effectively trapped by fluorine radicals (F$^{\bullet}$), which could convert high-energy free radicals into stable free radicals, thereby inhibiting the combustion process.[24,25] Furthermore, the heat-induced decomposition of PFPN can produce non-combustible gases like NH_3 and N_2, which would decrease the concentration of combustible gases and contribute to the overall flame retardancy of ether-based electrolyte and sulfur cathode.[26]

The ion conductivity of different electrolytes was tested using a conductivity meter, and the results are presented in Fig. 3a and Table 1. It is found that the ionic conductivities of the ether-based electrolytes decrease as the PFPN content increasing. The electrolytes with 0, 5%, 10%, 15%, 20% and 25% PFPN (PFPN-0, PFPN-5, PFPN-10, PFPN-15, PFPN-20 and PFPN-25) exhibit a decreased ionic conductivity of 11.9, 10.2, 9.63, 7.62, 5.87 and 4.45 mS cm^{-1}, respectively. The decreased ionic conductivity of the electrolytes contain PFPN can attribute to the high viscosity and low dielectric constant of PFPN.[27] However, when the amount of PFPN is excessive, the interaction force between the solvent molecules would increase, consequently increasing the resistance of Li^+ movement in the solution and declining the ionic conductivity of electrolyte. Linear Sweep Voltammetry (LSV) tests are performed to evaluate the electrochemical window of different electrolytes. As illustrated in Fig. 3b, the PFPN-0 electrolyte exhibits a electrochemical stability window of only 4.2 V. However, after adding PFPN into the ether electrolytes, the electrochemical stability windows of the all electrolytes have been widened. Especially for the PFPN-10 and PFPN-15 electrolytes, the oxidation currents both arise from ~5.0 V, manifesting that the PFPN addition can widen the electrochemical stability window of the ether-based electrolyte. The widened electrochemical stability windows of the ether-based electrolyte containing PFPN may be related to the strong electron-withdrawing effect of the fluorine atom.[28]

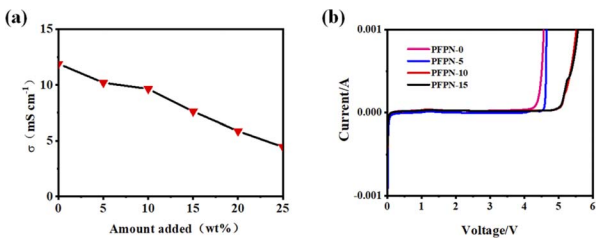

Fig. 3 (a) The ionic conductivity of the ether electrolytes with different amounts of PFPN; (b) LSV curves of the different electrolytes with a scan rate of 1.0 mV s^{-1}.

To evaluate the effect of PFPN additive on the interfacial stability of Li metal anode (LMA), Li–Li symmetric cells was tested with a discharge capacity of 0.5 mA h cm^{-2} and a constant current density of 0.5 mA cm^{-2}. Fig. 4a shows that the cell with PFPN-0 electrolyte occurs huge voltage fluctuation after 250 h with a sharp increase voltage polarization. With the increase of the amount of PFPN in the electrolytes, the cycle performance of Li–Li symmetrical cells have been greatly improved. Especially for the cell with PFPN-10 electrolyte, it exhibits the most stable cycle over 1000 h with the lowest polarization potential difference under 30 mV. These results suggest that PFPN promotes the formation of a stable SEI and facilitates the establishment of a more stable interface on the surface of Li anode, thereby enhancing the plating/stripping behavior of Li ion.[29] It is worth noting that when PFPN is added to 15 wt%, the performance of Li–Li symmetric batteries deteriorates. In order to investigate the underlying reasons, the impedances of the symmetric Li–Li cells with different electrolytes before cycling and the contact angle on separator for different electrolytes were both tested. Generally, the lower surface tension of electrolyte means better wettability.[30] It is found that with the increase of the amount of HFPN, the interfacial impedance of the Li–Li cells gradually increases (Fig. S3†), and the wettability of the electrolyte on separator gradually deteriorates (Fig. S4†). The poor wetting properties of the electrolyte and increased interfacial impedance may be related to the high viscosity of PFPN, which would lead to the decrease of ionic conductivity of the electrolyte (Fig. 3a) and the thickening of the SEI film. When the polarization of the Li–Li symmetric cells was measured at a constant current density of 1.0 mA cm^{-2} and a discharge capacity of 1.0 mA h cm^{-2}, the cell with PFPN-10 electrolyte also exhibited a more stable polarization potential difference (42 mV) and longer cycle life (1000 h) than the cell with PFPN-0 electrolyte, as shown in Fig. 4b.

Moreover, the electrochemical impedance spectroscopy (EIS) of the symmetric Li–Li cells with different electrolytes at 0.5 mA

Table 1 The ionic conductivity of electrolyte with different amount of PFPN

	PFPN-0	PFPN-5	PFPN-10	PFPN-15	PFPN-20	PFPN-25
σ (mS cm^{-1})	11.9	10.2	9.63	7.62	5.87	4.45

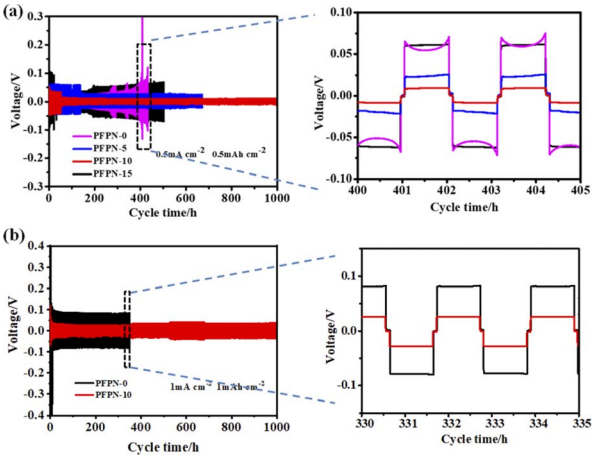

Fig. 4 Cycle performance curves and local amplification curves of Li–Li cells with different PFPN content: (a) 0.5 mA cm^{-2}, 0.5 mA h cm^{-2} and (b) 1.0 mA cm^{-2}, 1.0 mA h cm^{-2}.

cm^{-2} with 0.5 mA h cm^{-2} were performed to analyze the interfacial stability of Li anode surface at different cycling times. As shown in Fig. 5, the initial resistance values of the Li–Li cells with PFPN-0 and PFPN-10 were both large (about 150 Ω and 110 Ω, respectively), which mainly attributed to the lower Li ion conduction ability of the initially formed interface layer. Because the SEI film generated on the surface of Li anode is gradually stable and dense with cycling, hence the impedance of the Li–Li cells with PFPN-0 and PFPN-10 both gradually decrease during further cycling (80 to 200 h). However, for Li–Li symmetric cell with PFPN-0, the reaction between Li metal and electrolyte still continue during the further cycling, so the generated SEI film on the surface of the Li anode will become thicker or undergo damage, resulting in increased impedance. However, for the Li–Li symmetric cell with PFPN-10 electrolyte, PFPN may participate in film formation and generate LiF and Li_3N-rich SEI film with high ionic conductivity and high stability, therefore the resistance values of the Li–Li symmetric cell with PFPN-10 is stable without obvious change during 80–340 h. These results are also in agreement with the galvanostatic cycling performance of the symmetric Li–Li cells.

Furthermore, to explore the effects of PFPN on the morphology of lithium metal anode, the Li metal deposition morphology in the ether base electrolyte with/without PFPN after 50 cycles at 0.5 mA cm^{-2} and 0.5 mA h cm^{-2} is characterized by Scanning Electron Microscope (SEM). As shown in Fig. 6, for the cell with PFPN-0 electrolyte, the lithium anode exhibits a rough surface with noticeable dendritic protrusions and cracks, which will further aggravate the side reaction between the electrolyte and the lithium anode. Therefore, it is difficult to form stable SEI for lithium metal in PFPN-0 electrolyte, which would increase the risk of short circuits of the batteries. In contrast, the lithium anode with PFPN-10 electrolyte appears relatively smooth and flat surface with only few dendrites forming. These findings are consistent with the results of the Li–Li symmetrical cells and EIS measurements. The reason may be that the SEI formed by PFPN has a high interfacial energy, which can promote the planar deposition of lithium rather than vertical growth. This also facilitates the uniform deposition of lithium, resulting in the formation of a flat and dense electrolyte/electrode interface layer on the surface of the lithium anode, and effectively inhibiting the growth of lithium dendrites.[31,32]

In order to make clear the chemical compositions of the SEI layer of cycled Li anode with different electrolytes, the XPS tests of the Li anodes in Li–Li cells after 50 cycles of plating/stripping at 0.5 mA cm^{-2} and 0.5 mA h cm^{-2} are performed as shown in Fig. 7. By examining the C 1s, O 1s, F 1s, and N 1s spectra, the different components of the SEI layers of the different Li anodes can be identified. From Fig. 7, the XPS result showed the presence of lithium alkoxy (LiOR, 531.9 eV, O 1s), lithium carbonate (Li_2CO_3, 289.5 eV, C 1s and 533 eV, O 1s), lithium fluoride (LiF, 686 eV, F 1s) and lithium nitride (Li_3N, 399.5 eV) on the surfaces of all Li anodes with different electrolytes. It is worth noting that with the increase of PFPN content, the content of LiF and Li_3N in SEI layer both increases. It is well known that the high interface energy of LiF with Li is conducive to the diffusion of Li ions in parallel directions and the formation of uniform and dendrite-free deposition.[33] Furthermore, as a superionic conductor, Li_3N also can improve the conductivity of Li ion on the interface of solid electrolyte and reduce the polarization phenomenon.[34] Hence, with the increase of PFPN content, the formed SEI layer on the lithium surface became more dense and stable. However, it should be noted that the high resistance of LiF would cause the interface impedance of the battery increase,[35] resulting in a higher polarization voltage for Li–Li symmetric cells using the PFPN-15 electrolyte, which is consistent with the results in Fig. S3† and 4.

To further investigate the cycling stability of Li plating/stripping, the galvanostatic cycling test of the coin-type Li–

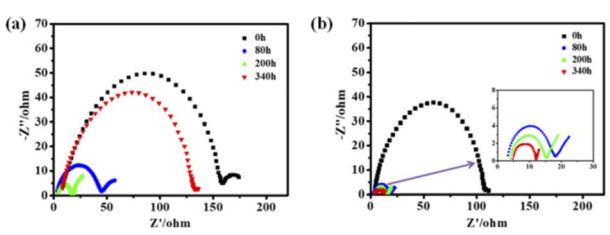

Fig. 5 Electrochemical impedance spectra of Li–Li cells at 0.5 mA cm^{-2} and 0.5 mA h cm^{-2} with different electrolyte: (a) PFPN-0, (b) PFPN-10.

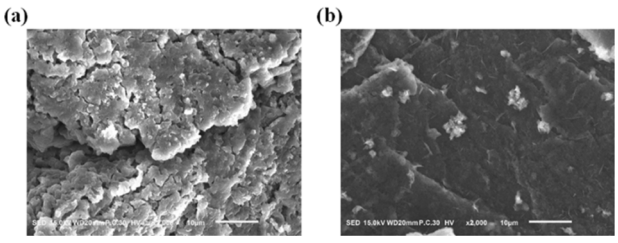

Fig. 6 SEM morphology of lithium anode in Li–Li cells after 50 cycles at 0.5 mA cm^{-2} and 0.5 mA h cm^{-2} with different electrolyte: (a) PFPN-0, (b) PFPN-10.

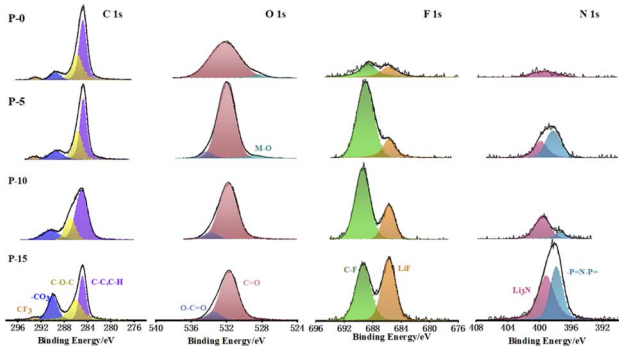

Fig. 7 XPS characterization test results of lithium anodes in Li–Li cells after 50 cycles at 0.5 mA cm^{-2} and 0.5 mA h cm^{-2} with different electrolytes.

Cu cells were constructed. The coulombic efficiency (CE) of the Li plating/stripping can be calculated from the ratio of the amount of stripped Li *versus* that of deposited Li in each cycle. In Fig. 7a and b, the CEs of Li–Cu cells in different electrolytes at 0.2 mA cm^{-2} and 0.5 mA cm^{-2} are compared. The Li–Cu cell with PFPN-10 electrolyte shows a more stable CE of 98% for 300 cycles at 0.2 mA cm^{-2} (Fig. 8a). In comparison, Li–Cu cell with PFPN-0 electrolyte presents a fluctuant CE and unstable cycling. When the current density is increased to 0.5 mA cm^{-2}, the Li–Cu cell with PFPN-10 electrolyte also shows a better cycling performance than the cell with PFPN-0 electrolyte (Fig. 8b). For the cell with PFPN-10 electrolyte, it can stable cycling for 150 cycles, while the cell with PFPN-0 electrolyte exhibits a rapid drop after about 30 cycles. This means that a significant amount of the Li deposited on the substrate reacted with the electrolyte and could not be recovered during the stripping process. Additionally, the Li–Cu cell using PFPN-0 electrolyte presents a larger voltage hysteresis than the cell with PFPN-10 electrolyte. The results indicate that the addition of PFPN in electrolyte is beneficial to the plating and stripping of Li.

In order to further investigate the Li metal deposition behavior, *ex situ* SEM observations were carried out on Cu electrodes in different electrolytes after 50 cycles at 0.2 mA cm^{-2}. As Fig. 8 shown, the deposited lithium on the Cu electrode surface exhibits significant uneven gaps when using PFPN-0 electrolyte, which is in agreement with the lower CE and shorter cycle life in Fig. 6. As using the PFPN-10 electrolyte, the deposited lithium on the Cu electrode surface shows an uniform, flat, and dense morphology, which can minimize the contact area between the electrode surface and the electrolyte, thereby reducing sustained parasitic reactions. The morphological analysis of the lithium deposition further confirms that the incorporation of PFPN in electrolyte can effectively enhance the plating and stripping behaviour of lithium while inhibiting the formation of lithium dendrite and "dead lithium".

In order to demonstrate the positive effect of PFPN on the electrochemical performance of Li–S cells, Li–S cells using PFPN-10 and PFPN-0 electrolytes were assembled respectively. As illustrated in Fig. 9a, the cell with PFPN-0 electrolyte demonstrates an initial specific capacity of 749.8 mA h g^{-1} and rapidly decreased to 549.2 mA h g^{-1} after 100 cycles at 0.2C, meaning that only 73.2% of the initial capacity is preserved. The deterioration may be attributed to the absence of a favorable solid-state electrolyte passivation layer on the cathode surface, which fails to suppress the shuttle effect of lithium polysulfides in the cell.[36] Encouragingly, the cell with PFPN-10 electrolyte shows a better cycling performance. The initial discharge capacity of the cell with PFPN-10 electrolyte is 1103.4 mA h g^{-1} at 0.2C, which is higher than that of the cell with PFPN-0 electrolyte. After 100 cycles, the capacity of the cell with PFPN-10 electrolyte still remains at 904.6 mA h g^{-1} with a capacity retention rate as high as 82% (Fig. 9a). In addition, the Li–S cell with PFPN-10 electrolyte also exhibits lower polarization voltage (Fig. 9b), which indicates that a more stable and denser passivation film with interfacial impedance formed on the cathode surface.

Furthermore, the rate performance of Li–S cells with PFPN-0 and PFPN-10 electrolytes are also tested. It is clear that the

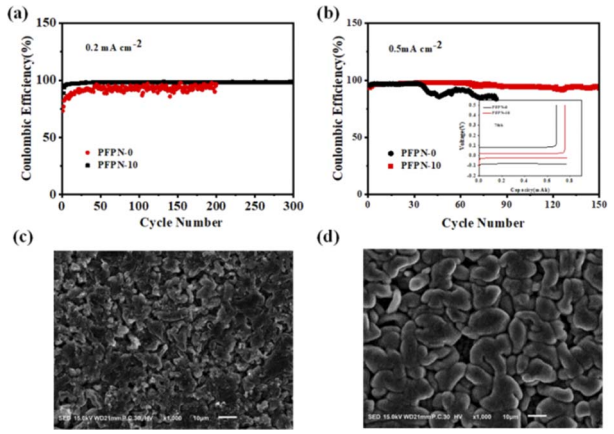

Fig. 8 CE of Li–Cu cells with PFPN-0 and PFPN-10 at different current densities: (a) 0.2 mA cm^{-2}, (b) 0.5 mA cm^{-2}; Cu electrode SEM morphology of Li–Cu cells after 50 cycles at 0.2 mA cm^{-2} with different electrolyte: (c) PFPN-0, (d) PFPN-10.

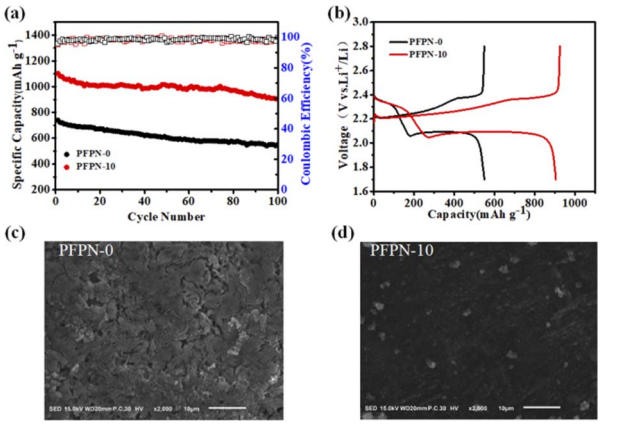

Fig. 9 (a) Cyclic performance and (b) charge–discharge curve at 100th cycle of Li–S batteries with PFPN-0 and PFPN-10 electrolyte (0.2C); SEM morphology of sulfur cathode in Li–S cells after 50 cycles at 0.2C with different electrolyte: (c) PFPN-0, (d) PFPN-10.

Li–S cells with PFPN-10 electrolyte delivered a better rate performance than that of the cell with PFPN-0 electrolyte (Fig. S5†). Even as the current density is elevated to 0.5C and 1.0C, the Li–S cells with PFPN-10 electrolyte can demonstrate a higher capacity of 881.2 and 720.6 mA h g^{-1}, respectively, while the Li–S cells with PFPN-0 electrolyte only can deliver a much lower capacity of 216.4 mA h g^{-1} and 127.7 mA h g^{-1}, respectively. All the above results demonstrate that Li–S cells with PFPN-10 electrolyte develop a good electrochemical performance, which is superior to Li–S cells with PFPN-0 electrolyte. These improvements can be attributed to the presence of F and P elements in the PFPN additive, which can oxidize on the cathode surface, forming a more stable and dense passivation film.[37] This film can effectively avoid the direct contact between the electrolyte and the electrode materials, which could avoid the side reaction between the electrode material and the electrolyte and reduce the electrolyte consumption, consequently improving the battery performance.

A comparative SEM analysis of the sulfur cathode surface after 50 cycles further substantiates the aforementioned observations and conclusions, as illustrated in Fig. 9c and d. The cathode surface in the PFPN-0 electrolyte exhibits uneven morphology and obvious cracks (Fig. 9c), which indicates that the porous structure exacerbates the side reactions between the electrode and the electrolyte and leads to the irreversible damage of the cathode structure. In contrast, the surface of sulfur cathode in PFPN-10 electrolyte is smooth and dense without any cracks (Fig. 9d). The reason may lie in the presence of PFPN, which can participate in the formation of a dense passivation film on the electrode surface, and then promote the uniform lithium plating/stripping process. Moreover, this passivation film effectively prevents electrolyte degradation and consumption of the sulfur cathode. As a result, the overall performance of the Li–S cell is improved.

4. Conclusions

In this study, in order to improve the safety performance of lithium–sulfur batteries, PFPN is utilized as both a film-forming electrolyte additive and a flame retardant additive for the ether-based electrolyte in Li–S batteries. It was found that PFPN not only has good flame retardant effect on ether-based electrolyte to improve the safety of electrolyte, but also can form a stable SEI film on the surface of lithium anode to enhance the safety of SEI. As a result, with the PFPN-10 ether-based electrolyte, Li–Cu and Li–S batteries all delivered a stable cycling performance with a high CE and a long-lifespan performance, which were all superior to the batteries using the ether-based electrolyte without PFPN. In a word, the ether-based electrolyte containing PFPN can effectively solve the problems about the flammable ether-based electrolyte and reactive lithium anode, which would be benefit for the development of the safe Li–S batteries.

Conflicts of interest

There are no conflicts to declare.

Acknowledgements

This work was financially supported by China Postdoctoral Science Foundation project (No. 2022M721374); China Petroleum & Chemical Corporation technology development project (No. 222066); the Natural Science Foundation of Jiangsu Province (No. bk20210767); Graduate Research and Innovation Projects of Jiangsu Province (No. SJCX22_1331 and No. SJCX22_1451).

References

1 C. P. Grey and D. S. Hall, Prospects for lithium-ion batteries and beyond-a 2030 vision, *Nat. Commun.*, 2020, **11**(1), 6279.
2 D. H. Liu, Z. Bai, M. Li, *et al.*, Developing high safety Li-metal anodes for future high-energy Li-metal batteries: strategies and perspectives, *Chem. Soc. Rev.*, 2020, **49**, 5407–5445.
3 M. Li, J. Lu, Z. Chen, *et al.*, 30 years of lithium-ion batteries, *Adv. Mater.*, 2018, **30**(33), 1800561.
4 L. Huang, T. Lu, G. Xu, *et al.*, Thermal runaway routes of large-format lithium-sulfur pouch cell batteries, *Joule*, 2022, **6**(4), 906–922.
5 G. Li, Z. Chen and J. Lu, Lithium-sulfur batteries for commercial applications, *Chem*, 2018, **4**(1), 3–7.
6 J. Liu, I. Salvation, K. Robert, *et al.*, A Comparison of Carbonate-Based and Ether-Based Electrolyte Systems for Lithium Metal Batteries, *J. Electrochem. Soc.*, 2023, **170**(1), 010535.
7 J. Wang, The opinions for lithium sulfur battery, *Energy Storage Sci. Technol.*, 2020, **9**(01), 1–4.
8 Z. Hou, J. Zhang, W. Wang, *et al.*, Towards high-performance lithium metal anodes *via* the modification of solid electrolyte interphases, *J. Energy Chem.*, 2020, **45**, 7–17.
9 J. Janek and W. G. Zeier, A solid future for battery development, *Nat. Energy*, 2016, 141.
10 C. Shuru, Z. Jianming, Y. Lu, *et al.*, High-efficiency lithium metal batteries with fire-retardant electrolytes, *Joule*, 2018, **2**(8), 1548–1558.
11 X. Tang, S. Y. Lv, K. Jiang, *et al.*, Recent development of ionic liquid-based electrolytes in lithium-ion batteries, *J. Power Sources*, 2022, 542.
12 Y. Zhao, T. Zhou, T. Ashirov, *et al.*, Fluorinated ether electrolyte with controlled solvation structure for high voltage lithium metal batteries, *Nat. Commun.*, 2022, **13**(1), 2575.
13 L. Zhang, Y. Huang, H. Fan, *et al.*, Flame-retardant electrolyte solution for dual-ion batteries, *ACS Appl. Energy Mater.*, 2019, **2**(2), 1363–1370.
14 X. Wang, W. He, H. Xue, *et al.*, A nonflammable phosphate based localized high-concentration electrolyte for safe and high-voltage lithium metal batteries, *Sustainable Energy Fuels*, 2022, **6**(5), 1281–1288.
15 Z. Yu, J. Zhang, C. Wang, *et al.*, Flame-retardant concentrated electrolyte enabling a LiF-rich solid electrolyte interface to improve cycle performance of wide-temperature lithium-sulfur batteries, *J. Energy Chem.*, 2020, **51**, 154–160.

16 H. L. Wu, Y. H. Chong, H. C. Ong, *et al.*, Thermal stability of modified lithium-ion battery electrolyte by flame retardant, tris(2,2,2-trifluoroethyl)phosphite, *J. Therm. Anal. Calorim.*, 2021, **147**(6), 4245–4252.
17 X. Li, W. Li, L. Chen, *et al.*, Ethoxy(pentafluoro) cyclotriphosphazene (PFPN) as a multi-functional flame retardant electrolyte additive for lithium-ion batteries, *J. Power Sources*, 2018, **378**, 707–716.
18 L. Chen, Q. Nian, D. Ruan, *et al.*, High-safety and high-efficiency electrolyte design for 4.6 V-class lithium-ion batteries with a non-solvating flame-retardant, *Chem. Sci.*, 2022, **14**(5), 1184–1193.
19 Y. Li, Y. An, Y. Tian, *et al.*, High-safety and high-voltage lithium metal batteries enabled by a nonflammable ether-based electrolyte with phosphazene as a cosolvent, *ACS Appl. Mater. Interfaces*, 2021, **13**(8), 10141–10148.
20 H. Fei, Y. An, J. Feng, *et al.*, Enhancing the safety and electrochemical performance of ether based lithium sulfur battery by introducing an efficient flame retarding additive, *RSC Adv.*, 2016, **6**(58), 53560–53565.
21 C. Qu, Y. Chen, X. Yang, *et al.*, $LiNO_3$-free electrolyte for Li-S battery: a solvent of choice with low Ksp of polysulfide and low dendrite of lithium, *Nano Energy*, 2017, **39**, 262–272.
22 W. Wang, H. Hu, X. Zeng, *et al.*, Comprehensive insight into the probability of cyclotriphosphazene derivatives as the functional electrolyte additives in lithium-ion batteries: which is better and why?, *ACS Appl. Energy Mater.*, 2021, **4**(7), 7101–7111.
23 Z. L. Shao, J. Liang, S. Hu, *et al.*, Studies on heat decomposition and combustion of polyethylene modified by flame retardants, *Fire Saf. Sci.*, 1998, (01), 40–44.
24 H. H. Kim, M. J. Sim, J. C. Lee, *et al.*, The effects of chemical structure for phosphorus-nitrogen flame retardants on flame retardant mechanisms, *J. Mater. Sci.*, 2023, **58**(15), 6850–6864.
25 G. Xu, C. Pang, B. Chen, *et al.*, Prescribing functional additives for treating the poor performances of high-voltage (5 V-class) $LiNi_{0.5}Mn_{1.5}O_4$/MCMB Li-ion batteries, *Adv. Energy Mater.*, 2018, **8**, 1701398.
26 C. Bao, Y. Guo, B. Yuan, *et al.*, Functionalized graphene oxide for fire safety applications of polymers: a combination of condensed phase flame retardant strategies, *J. Mater. Chem.*, 2012, **22**(43), 23057.
27 C. Bao, Y. Guo, B. Yuan, *et al.*, Functionalized graphene oxide for fire safety applications of polymers: a combination of condensed phase flame retardant strategies, *J. Mater. Chem.*, 2012, **22**(43), 23057.
28 Q. Liu, Z. Chen, Y. Liu, *et al.*, Cooperative stabilization of bi-electrodes with robust interphases for high-voltage lithium-metal batteries, *Energy Storage Mater.*, 2021, **37**, 521–529.
29 X. Zhu, X. Jiang, X. Ai, *et al.*, Bis(2,2,2-trifluoroethyl) ethylphosphonate as novel high-efficient flame retardant additive for safer lithium-ion battery, *Electrochim. Acta*, 2015, **165**, 67–71.
30 D. Lu, S. Zhang, J. Li, *et al.*, Transformed solvation structure of noncoordinating flame-Retardant assisted propylene carbonate enabling high voltage Li-ion batteries with high safety and long cyclability, *Adv. Energy Mater.*, 2023, **13**, 2300684.
31 Y. Lu, Z. Tu and L. A. Archer, Stable lithium electrodeposition in liquid and nanoporous solid electrolytes, *Nat. Mater.*, 2014, **13**(10), 961–969.
32 X. Fan, X. Ji, L. Chen, *et al.*, All-temperature batteries enabled by fluorinated electrolytes with non-polar solvents, *Nat. Energy*, 2019, **4**(10), 882–890.
33 S. Zhang, X. Zhuang, X. Du, *et al.*, A novel potassium salt regulated solvation chemistry enabling excellent Li-anode protection in carbonate electrolytes, *Adv. Mater.*, 2023, **35**, 2301312.
34 Y. Ma, J. Wan, Y. Yang, *et al.*, Scalable, ultrathin, and high-temperature-resistant solid polymer electrolytes for energy-dense lithium metal batteries, *Adv. Energy Mater.*, 2022, **12**(15), 2103720.
35 C. Bolli, A. Guéguen, M. A. Mendez, *et al.*, Operando monitoring of F-formation in lithium ion batteries, *Chem. Mater.*, 2019, **31**(4), 1258–1267.
36 C. Yan, X. Q. Zhang, J. Q. Huang, *et al.*, Lithium-anode protection in lithium-sulfur batteries, *Trends Chem.*, 2019, **1**(7), 693–704.
37 Y. Ji, P. Zhang, M. Lin, *et al.*, Toward a stable electrochemical interphase with enhanced safety on high-voltage $LiCoO_2$ cathode: a case of phosphazene additives, *J. Power Sources*, 2017, **359**, 391–399.